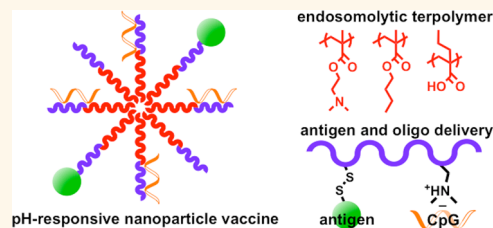


# pH-Responsive Nanoparticle Vaccines for Dual-Delivery of Antigens and Immunostimulatory Oligonucleotides

John T. Wilson, Salka Keller, Matthew J. Manganiello, Connie Cheng, Chen-Chang Lee, Chinonso Opara, Anthony Convertine, and Patrick S. Stayton\*

Department of Bioengineering, University of Washington, Seattle, Washington 98195, United States

**ABSTRACT** Protein subunit vaccines offer important potential advantages over live vaccine vectors but generally elicit weaker and shorter-lived cellular immune responses. Here we investigate the use of pH-responsive, endosomolytic polymer nanoparticles that were originally developed for RNA delivery as vaccine delivery vehicles for enhancing cellular and humoral immune responses. Micellar nanoparticles were assembled from amphiphilic diblock copolymers composed of an amphotropic core-forming block and a redesigned polycationic corona block doped with thiol-reactive pyridyl disulfide groups to enable dual-delivery of antigens and immunostimulatory CpG oligodeoxynucleotide (CpG ODN) adjuvants. Polymers assembled into 23 nm particles with simultaneous packaging of CpG ODN and a thiolated protein antigen, ovalbumin (ova). Conjugation of ova to nanoparticles significantly enhanced antigen cross-presentation *in vitro* relative to free ova or an unconjugated, physical mixture of the parent compounds. Subcutaneous vaccination of mice with ova–nanoparticle conjugates elicited a significantly higher CD8<sup>+</sup> T cell response (0.5% IFN- $\gamma$ <sup>+</sup> of CD8<sup>+</sup>) compared to mice vaccinated with free ova or a physical mixture of the two components. Significantly, immunization with ova–nanoparticle conjugates electrostatically complexed with CpG ODN (dual-delivery) enhanced CD8<sup>+</sup> T cell responses (3.4% IFN- $\gamma$ <sup>+</sup> of CD8<sup>+</sup>) 7-, 18-, and 8-fold relative to immunization with conjugates, ova administered with free CpG, or a formulation containing free ova and CpG complexed to micelles, respectively. Similarly, dual-delivery carriers significantly increased CD4<sup>+</sup> IFN- $\gamma$ <sup>+</sup> (Th1) responses and elicited a balanced IgG1/IgG2c antibody response. Intradermal administration further augmented cellular immune responses, with dual-delivery carriers inducing ~7% antigen-specific CD8<sup>+</sup> T cells. This work demonstrates the ability of pH-responsive, endosomolytic nanoparticles to actively promote antigen cross-presentation and augment cellular and humoral immune responses *via* dual-delivery of protein antigens and CpG ODN. Hence, pH-responsive polymeric nanoparticles offer promise as a delivery platform for protein subunit vaccines.



**KEYWORDS:** vaccine · pH-responsive polymer · micelle · CpG adjuvant · endosomal escape · antigen cross-presentation

Synthetic subunit vaccines offer potential benefits over live or attenuated vaccine vectors in some disease applications, including improved safety, reduced cost, ease of manufacturability, and control over the antigen specificity of the immune response.<sup>1,2</sup> General limitations of protein subunit vaccines, however, include typically weak and short-lived humoral and cellular immune responses.<sup>3–6</sup> It has been particularly challenging to elicit CD8<sup>+</sup> cytotoxic T lymphocyte (CTL) responses, which are thought to be critical for effective vaccination against diseases such as HIV, hepatitis C, and malaria, as well as in cancer immunotherapy.<sup>7,8</sup> Underlying this difficulty are key delivery challenges, including transport and targeting of the vaccine to the correct antigen-presenting cells (APCs) and cross-presentation of exogenously

administered antigens on major histocompatibility complex class I (MHC-I) of dendritic cells (DCs).<sup>5–7,9,10</sup> Soluble protein antigen endocytosed by APCs is generally degraded in specialized endo/lysosomal compartments, resulting in preferential MHC class II presentation and subsequent generation of CD4<sup>+</sup> helper T cell responses.<sup>5,6</sup> By contrast, engineered viral vectors have been developed that induce robust CTL responses, due in part to expression of antigen in the cytosol with subsequent entry to the endogenous MHC class I antigen presentation pathway.<sup>7,11</sup> Safety and specificity concerns regarding the use of viral vectors continue to drive work aimed at improving subunit vaccine efficacies.<sup>6,7,11</sup>

A number of investigators have engineered pathogen-inspired synthetic vaccines to enhance antigen cross-presentation.<sup>3,5,6,12–16</sup>

\* Address correspondence to stayton@u.washington.edu.

Received for review November 25, 2012 and accepted April 16, 2013.

Published online April 16, 2013  
10.1021/nn305466z

© 2013 American Chemical Society

A common approach has been to use micro- and nanoparticles as a platform for co-delivery of antigen and immunostimulatory molecules to the same APC, which can promote cross-presentation and help elicit a broader cellular response.<sup>12,17–21</sup> Additionally, a number of pathogenic organisms utilize pH-dependent mechanisms to facilitate their escape from endo/lysosomal trafficking pathways into the cytosol.<sup>22,23</sup> By analogy, our group has postulated that synthetic materials with pH-dependent membrane-destabilizing characteristics provide a versatile strategy for enhancing delivery of protein antigens into the cytosolic MHC-I antigen presentation pathway. We have previously demonstrated that covalent tethering of antigen to the pH-responsive polymer poly(propylacrylic acid) can enhance intracellular antigen accumulation, thereby increasing MHC-I presentation and enhancing CD8<sup>+</sup> T cell responses *in vivo*.<sup>24,25</sup>

While a number of nanoparticle delivery systems have been developed that enable dual-delivery of antigen and immunostimulatory adjuvants, there are relatively few below 100 nm in diameter and, to the best of our knowledge, none within this size range that also incorporate endosomal escape functionalities to actively alter intracellular trafficking. Here we build upon a recently described pH-responsive, endosomolytic polymer micelle design, initially developed for siRNA delivery,<sup>26,27</sup> to construct a subunit vaccine that facilitates concomitant delivery of antigen and immunostimulatory oligonucleotide adjuvants on a single nanoparticle platform (Figure 1). To enable the application of this micellar carrier for vaccine delivery, we have introduced pyridyl disulfide groups into the cationic corona for reversible conjugation of protein antigens to be carried together with an electrostatically complexed nucleic acid species. The diblock copolymers self-assemble into micellar nanoparticles ~30 nm in diameter and demonstrate potent pH-dependent membrane destabilizing activity. As an adjuvant, we have used an oligodeoxyribonucleotide (ODN) containing an unmethylated cytosine-phosphate-guanine (CpG) sequence that mimics motifs found in bacterial and viral DNA. CpG ODNs bind the endosomal receptor TLR9, initiating an innate immune response characterized by the production of pro-inflammatory and Th1 cytokines that promote CTL and CD4<sup>+</sup> Th1 activation.<sup>28,29</sup> Here we show that this micelle carrier facilitates loading of both a protein antigen (ovalbumin) and CpG ODN, and that dual-delivery synergistically enhances humoral and cellular immune responses. This represents the first use of such pH-responsive endosomolytic polymeric nanoparticles to enhance the intracellular delivery of a protein antigen and demonstrates the unique capability of these carriers to actively promote antigen cross-presentation *via* increased cytosolic delivery and enhance antigen-specific immune responses *via*

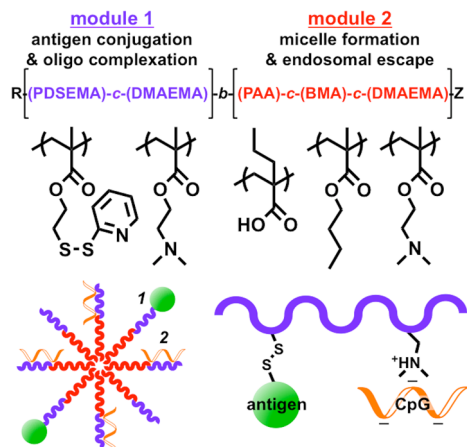


**Figure 1.** Nanoparticle vaccines based on pH-responsive polymers for dual-delivery of antigen and oligonucleotides. Amphiphilic diblock copolymers with two multifunctional modules were synthesized by reversible addition–fragmentation chain transfer (RAFT) polymerization. The hydrophilic and cationic first block was composed of DMAEMA for electrostatic complexation of oligonucleotide adjuvants (CpG ODN) and a small percentage of PDSEMA for conjugation of thiol-bearing antigens (ovalbumin) via disulfide exchange. The hydrophobic and endosomolytic second block drives micelle assembly and promotes cytosolic antigen delivery.

dual-delivery of antigen and an endosomal-acting oligonucleotide adjuvant.

## RESULTS AND DISCUSSION

**Synthesis of pH-Responsive Nanocarriers for Dual-Delivery of Antigen and CpG ODN.** RAFT polymerization was employed to synthesize amphiphilic diblock copolymers comprising a polycation-rich block that incorporated pyridyl disulfide (PDS) functional groups and a hydrophobic, endosomolytic segment to induce micelle assembly and promote antigen cross-presentation *via* enhanced cytosolic delivery (Figure 1). The first module was achieved through synthesis of a new copolymer composed primarily of the cationic monomer dimethylaminoethyl methacrylate (DMAEMA) (97%) doped with a small percentage (3%) of PDS ethyl methacrylate (PDSEMA). The number average molecular weight ( $M_n$ ) of the copolymer was 10 kDa, and the polydispersity index (PDI) was 1.1. Using poly-(DMAEMA-co-PDSEMA) as a macro-chain transfer agent (mCTA), a second terpolymer amphotolyte block was polymerized with DMAEMA, propylacrylic acid (PAA), and butyl methacrylate (BMA).<sup>26</sup> The  $M_n$  of this second block was 21.5 kDa with a composition of 34% DMAEMA, 27% PAA, and 39% BMA. The PDI of 1.9 for the diblock copolymer is high for a true RAFT-based polymerization, likely due to the sterically hindered PAA monomer which slows chain propagation resulting in hybrid behavior between conventional and living free-radical polymerization.<sup>30,31</sup> Nonetheless, a clear shift in the molecular weight distribution is observed (see Supporting Information, Figure S2), indicating the formation of the desired diblock copolymer

architecture. Dynamic light scattering (DLS) of polymers in aqueous solution (PBS, pH 7.4) revealed particles with an average diameter of  $23.4 \pm 3.3$  nm, indicating the assembly of a micellar architecture driven by the hydrophobic core-forming pH-responsive block. Static light scattering measurements indicated a micelle molecular weight of  $\sim 2610$  kDa and, therefore, an aggregation number of  $\sim 80$  polymer chains per micelle.

The ability of micellar nanoparticles to carry ovalbumin (ova) and/or CpG ODN was next assessed. In order to identify the relationship (mixed, conjugated, or electrostatically associated) between the different components of the formulation (polymer, ova, and CpG), the following nomenclature was adopted and used henceforth. Free ovalbumin will be referred to as "ova", free ova mixed with CpG as "ova+CpG", ova-polymer conjugates as "ova-pol", free ova mixed with free polymer as "ova+pol", ova-polymer conjugates electrostatically associated with CpG as "ova-pol/CpG", and free ova mixed with polymer electrostatically associated with CpG as "ova+pol/CpG". To enable conjugation of ova to the PDS groups, thiols were first introduced using 2-iminothiolane (3–5 thiols/ova).<sup>25,32</sup> Conjugation of ova to polymer (ova-pol) was evaluated using SDS-PAGE to monitor the shift of fluorescently labeled ova to higher molecular weights, accompanied by disappearance of the free protein band. Reaction of thiolated ova and polymer at a 20:1 polymer/ova ratio resulted in >95% conjugation of protein to the micelles as determined by SDS-PAGE (Figure 2a). By contrast, conjugation was not observed upon mixing nonthiolated, native ova with polymer (ova+pol), likely owing to the low accessibility of free cysteine residues present in ovalbumin.<sup>33</sup> Incubation of nanoparticle–ova conjugates with cytosolic levels of glutathione (10 mM)<sup>34</sup> resulted in complete liberation of ova from the carrier (Figure 2a), a property which has been shown to improve delivery of conjugate-based vaccines.<sup>35</sup> It should be noted that, upon conjugation to the polymer, the ova band becomes distributed over a broad range of molecular weights. This is most likely reflective of both the polydispersity of the polymeric carrier, which also displays a band over a range of molecular weights (Figure S3, Supporting Information), as well as heterogeneity in the number of conjugation events per ova or polymer chain (e.g., multiple ova per polymer chain or multiple polymer chains per ova). Nonetheless, no significant change in particle size was observed upon antigen conjugation via DLS ( $25.1 \pm 5.2$  nm), suggesting maintenance of micellar structure and minimal particle cross-linking or aggregation. Conjugates were subsequently incubated with CpG ODN at various  $\pm$ charge ratios (ova-pol/CpG), defined as the molar ratio of protonated DMAEMA tertiary amines in the first block (assuming 50% protonation at physiological pH) and phosphate groups along the CpG

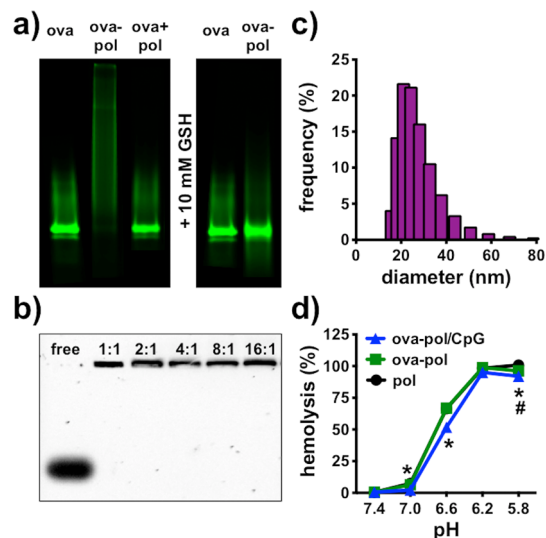


**Figure 2.** pH-responsive micellar nanocarriers for dual-delivery of antigen and oligonucleotides. (a) SDS-PAGE of fluorescently labeled ovalbumin (ova), nanoparticle–ova conjugates at a polymer/ova molar ratio of 20:1 (ova-pol), and a physical mixture of ova and polymer (ova+pol). Incubation of conjugates with intracellular concentrations of glutathione (GSH) liberates ova from the carrier. (b) Agarose gel electrophoresis of ova–nanoparticle conjugates incubated with CpG ODN1826 at various positive/negative charge ratios. (c) Representative size distribution (number average) measured by dynamic light scattering (DLS) of ova-pol/CpG complexes at a 4:1 charge ratio. (d) Erythrocyte lysis assay demonstrating pH-dependent membrane destabilizing activity of the diblock copolymer micelles (pol), nanoparticle–ova conjugate (ova-pol), and conjugate complexed with CpG ODN (ova-pol/CpG). Concentrations are normalized to  $2.5 \mu\text{g/mL}$  polymer and data represent mean  $\pm$  SD ( $n = 4$ ); \* $p < 0.05$ : ova-pol/CpG vs pol and ova-pol; # $p < 0.05$ : ova-pol vs pol by ANOVA with Tukey's post-hoc test.

backbone. An agarose gel electrophoretic shift assay was performed to determine the charge ratio where polymers were able to bind and completely neutralize the negative charges of CpG. At charge ratios of 1:1 and above, CpG ODN was completely complexed to polymeric carriers, as indicated by the disappearance of a free CpG band and the lack of CpG migration toward the cathode (Figure 2b). However, at charge ratios of 1:1 and 2:1, particle size increased dramatically ( $\sim 1000$ – $3000$  nm), likely as a result of colloidal destabilization and/or cross-bridge formation associated with addition of CpG ODN. Increasing the charge ratio to 4:1 mitigated this effect with resultant particles returning to  $26.7 \pm 6.0$  nm (Figure 2c), a size comparable to smaller viruses (e.g., adeno-associated virus, pox virus, polio virus) that is also amenable to sterile filtration.<sup>36</sup> Consistent with our previous reports,<sup>27</sup> nanoparticles demonstrated potent pH-dependent membrane disruptive properties in an erythrocyte lysis assay (Figure 2d), thereby mimicking the mechanism of endosomal escape utilized by a number of pathogens (e.g., influenza, adenovirus, *Listeria monocytogenes*). This response was only modestly inhibited by conjugation of ova or electrostatic complexation of CpG at a 4:1 charge ratio. This nanoparticle

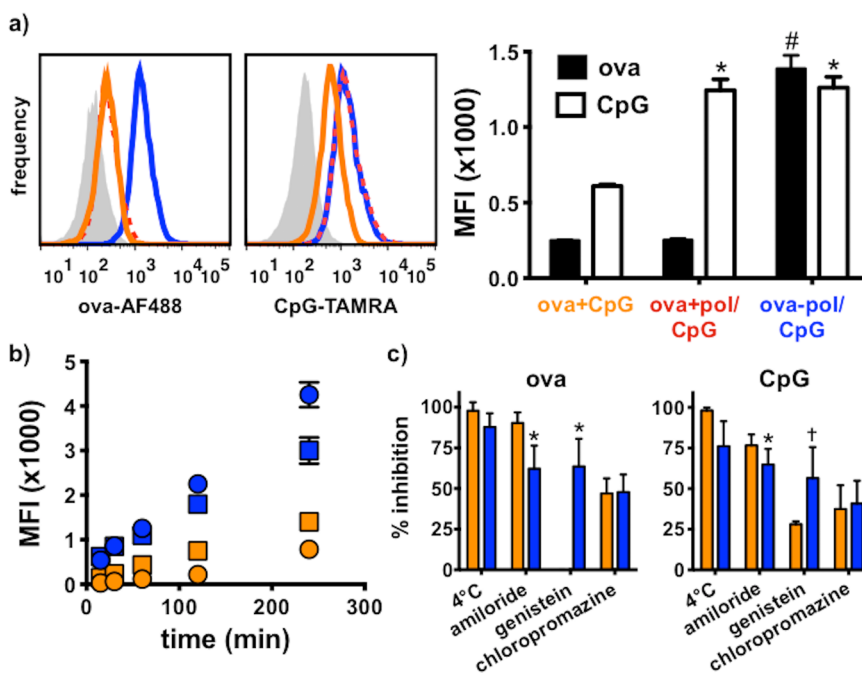


**Figure 3.** Dual-delivery nanoparticles enhance uptake of ova and CpG by dendritic cells through multiple endocytic pathways. (a) Uptake of AlexaFluor488-labeled ova and TAMRA-labeled CpG measured by flow cytometry after 1 h incubation at 37 °C. Left: Representative flow cytometry histograms of DC2.4 cells untreated (gray fill) or incubated with ova mixed with CpG (ova+CpG; orange line), dual-delivery carriers (ova-pol/CpG; blue line), and ova mixed with CpG complexed to polymer (ova+pol/CpG; dotted red line). Right: Median fluorescent intensity (MFI) for each treatment group (mean  $\pm$  SD,  $n = 3$ ; \* $p < 0.05$  ova+pol/CpG and ova-pol/CpG vs ova+CpG, # $p < 0.05$  ova-pol/CpG vs ova+CpG and ova+pol/CpG by ANOVA with Tukey's post-hoc test). (b) Kinetics of uptake for ova (circles) and CpG (squares) either delivered free (ova+CpG; orange) or as part of the dual-delivery (ova-pol/CpG) construct (blue; mean  $\pm$  SD,  $n = 3$ ). At each time point, the MFI corresponding to both ova and CpG are statistically higher ( $p < 0.05$  by student's t test) in the ova-pol/CpG (blue) treatment group. (c) Inhibition of ova (left) and CpG (right) uptake upon incubation at 4 °C or in the presence of the indicated inhibitors for 1 h at 37 °C expressed as a percentage of control after subtracting background MFI. Orange bars represent ova mixed with CpG (ova+CpG), and blue bars represent dual-delivery carriers (ova-pol/CpG). Genistein treatment did not significantly ( $p \gg 0.05$ ) change ova uptake in the ova+CpG (orange) group relative to untreated control; the average percent inhibition of ova in this group was slightly negative ( $-5\%$ ), and this data point has been eliminated for clarity. Data are expressed as the mean  $\pm$  SD from four independent experiments; \* $p < 0.05$ , †  $< 0.1$  ova-pol/CpG (blue) vs ova+CpG (orange) by student's t test for a given treatment group.

formulation, comprising an average of  $\sim 80$  polymer chains,  $\sim 4$  ova molecules, and  $\sim 30$  strands of CpG ODN, was chosen for all subsequent investigations.

**Nanoparticle Carriers Enhance Intracellular Uptake of Antigen and CpG ODN.** By mimicking the intracellular uptake of antigen and immunostimulatory DNA that occurs during bacterial and viral infections, the co-delivery of antigen with CpG ODN has been shown to enhance immune responses to vaccines.<sup>12,17–21,37,38</sup> To demonstrate that carriers promote uptake of both antigen and CpG, flow cytometry was used to investigate the internalization of AlexaFluor488-labeled ova and TAMRA-labeled CpG in DC2.4 cells, a dendritic cell line.<sup>39</sup> After 1 h incubation with particles carrying ova and CpG (ova-pol/CpG), ova and CpG uptake were enhanced 5.5- and 2.5-fold, respectively, over the parental formulation of ova mixed with CpG (ova+CpG; Figure 3a). A physical mixture of free ova and CpG complexed to particles (ova+pol/CpG) did not increase internalization of ova, demonstrating a dependence on direct conjugation in enhanced uptake. Additionally, nanoparticle delivery increased the initial rate of uptake, defined as the change in median fluorescence intensity (MFI) of the

DC2.4 cell population per minute over the first 240 min of incubation, 5-fold and 1.9-fold for ova and CpG, respectively (Figure 3b). These data provide evidence of dual-delivery of a protein antigen and an oligonucleotide adjuvant on a common synthetic platform.

To elucidate the mechanism through which ova and CpG are endocytosed by DC2.4 cells, treatments were performed at 4 °C or in the presence of the macropinocytosis inhibitor amiloride,<sup>40</sup> the caveolae inhibitor genistein,<sup>41</sup> or the inhibitor of clathrin-mediated endocytosis, chloropromazine.<sup>42</sup> Uptake of CpG and ova associated with the carrier (ova-pol/CpG) was nearly completely abrogated at 4 °C (Figure 3c), demonstrating the energy dependence of uptake and that particle internalization is not mediated by non-specific membrane fusion or translocation. Uptake of CpG and ova on carriers was inhibited to similar extents by genistein, amiloride, and chloropromazine, indicating that multiple endocytic pathways are likely involved in the internalization of nanoparticles. It is notable that the uptake of CpG and ova on carriers was reduced by comparable degrees in all treatment groups, further suggesting that both species

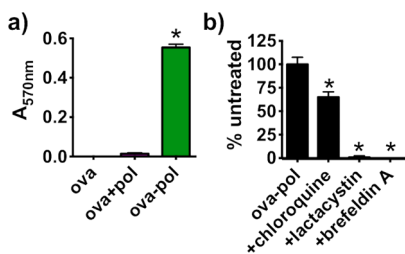


**Figure 4. Conjugation of antigen to polymeric carriers enhances MHC class I antigen presentation.** (a) DC2.4 cells were incubated with ova (1  $\mu$ g/mL), ova–nanoparticle conjugates (ova-pol), or a mixture of micelles and nonthiolated ova (ova+pol) for 4 h and subsequently cocultured for 18–20 h with B3Z T cell hybridomas which produce  $\beta$ -galactosidase upon recognition of ova<sub>257–264</sub> (SIINFEKL) presented on the murine H-2K<sup>b</sup> MHC class molecule.  $\beta$ -Galactosidase was subsequently detected using a lysis buffer containing a colorimetric substrate with an absorbance at 570 nm (mean  $\pm$  SD,  $n = 4$ , \* $p < 0.05$  ova-pol vs ova+pol and ova by ANOVA with Tukey's post-hoc test. (b) Enhanced MHC-I presentation was inhibited by addition of chloroquine and completely abrogated with lactacystin and brefeldin A, indicating that polymer-mediated cross-presentation is dependent on endosomal acidification, proteosomal processing, and transport of MHC-I/peptide complexes from the endoplasmic reticulum to the cell surface (mean  $\pm$  SD,  $n = 4$ , \* $p < 0.05$  vs ova-pol by Student's *t* test).

are entering cells together. It is also notable that free ova does not enter dendritic cells through caveolae, consistent with previous studies demonstrating that ova uptake is mediated by macropinocytosis and the mannose receptor (clathrin),<sup>43–45</sup> whereas ova conjugated to nanocarriers can utilize caveolae as an alternative internalization route.

**Polymeric Delivery of Antigen Enhances MHC-I Presentation in a B3Z T Cell Activation Assay.** A coculture assay was used to characterize antigen delivery into the MHC class I processing pathway. DC2.4 cells were incubated with the indicated ova-containing formulations and subsequently cocultured with a B3Z T cell hybridoma which produces  $\beta$ -galactosidase upon recognition of ova<sub>257–264</sub> (SIINFEKL) presented on the murine H-2K<sup>b</sup> MHC molecule. Conjugation of ova to pH-responsive carriers dramatically increased class I antigen presentation relative to soluble ova, which was detected at negligible levels over background (Figure 4a). Additionally, a physical mixture of nonthiolated ova and polymer did not significantly enhance antigen presentation, further demonstrating the requirement for antigen conjugation. While noncovalent interactions (e.g., electrostatic interactions, hydrogen bonding) between the micelle and ova are possible, these data, combined with the cellular uptake data described previously (Figure 3), strongly suggest that such interactions, if present, are weak and/or transient and, therefore, likely play a negligible role in enhancing the intracellular delivery of ova.

To probe the mechanism of polymer-mediated cross-presentation, DC2.4 cells were treated with chloroquine, an inhibitor of endosomal acidification, lactacystin, a proteosome inhibitor, and brefeldin A, which inhibits

transport of assembled MHC-I/peptide complexes from the endoplasmic reticulum (ER) to the cell surface. Treatment with chloroquine resulted in a 35% reduction in antigen presentation, while lactacystin and brefeldin A completely abrogated the response (Figure 4b). The persistence of some class I presentation in the presence of chloroquine is likely due to incomplete inhibition of endosomal acidification,<sup>46</sup> resulting in elevated pH values where polymers nonetheless still maintain membrane-disruptive capabilities. Treatment of antigen-presenting cells with chloroquine has also been associated with increased cross-presentation of endocytosed antigen due to membrane leakage and reduced proteolytic antigen degradation.<sup>47</sup> However, a dependence on endosomal acidification as well as proteosomal processing and transport from the ER suggests that the acidic milieu of endosomal trafficking facilitates polymer-mediated delivery of antigen to the cytosol for processing *via* the classical/endogenous class I presentation pathway.

**Nanoparticle–Antigen Conjugates Enhance CD8<sup>+</sup> T Cell and Antibody Responses *In Vivo*.** To evaluate the capacity of conjugates to enhance CD8<sup>+</sup> T cell responses *in vivo*, C57BL/6 mice were injected subcutaneously with free ova (ova), nanoparticle–ova conjugate (ova-pol), or a physical mixture of micelles and ova (ova+pol) in formulations containing 25  $\mu$ g ova and/or 360  $\mu$ g of polymer. A booster injection of the same formulation was given on day 21. Mice were sacrificed 1 week later, and the CD8<sup>+</sup> T cell response was determined through *ex vivo* stimulation of isolated splenocytes with the immunodominant class I ova epitope (SIINFEKL). The quantification of INF- $\gamma$  producing cells was performed using intracellular cytokine staining and ELISPOT. Immunization with polymer–ova conjugates resulted in 0.5  $\pm$  0.13% ova-specific CD8<sup>+</sup> T cells (% IFN- $\gamma$ <sup>+</sup> of CD8<sup>+</sup>) as measured by intracellular cytokine staining (Figure 5a), a significantly ( $p < 0.05$ ) higher response than elicited with free ova (0.02%) or a physical mixture of particles and ova (0.03%). Quantification of the CD8<sup>+</sup> T cell response using IFN- $\gamma$  ELISPOT (Figure 5b) corroborated these findings, with conjugates (200  $\pm$  60 spot forming cells (SFC)/ $1 \times 10^6$ ) generating a 17- and 90-fold increase in response relative to the physical mixture and free ova, respectively. This is consistent with the need for intracellular colocalization of polymer and antigen. Further studies will be necessary to elucidate the mechanisms through which conjugates mediate enhanced cross-presentation *in vivo* and the cell types involved.

Immunization with ova–nanoparticle conjugates (ova-pol) enhanced IgG1 and IgG2c antibody titer  $\sim$ 1500- and  $\sim$ 300-fold, respectively, over antigen alone (Figure 5c; note that titer values are plotted on a log<sub>10</sub> axis). However, the physical mixture of particles and ova (ova+pol) also increased antibody titer over free ova, albeit to a lesser extent ( $\sim$ 30-fold for IgG1 and  $\sim$ 150-fold for IgG2c). The difference in titer between

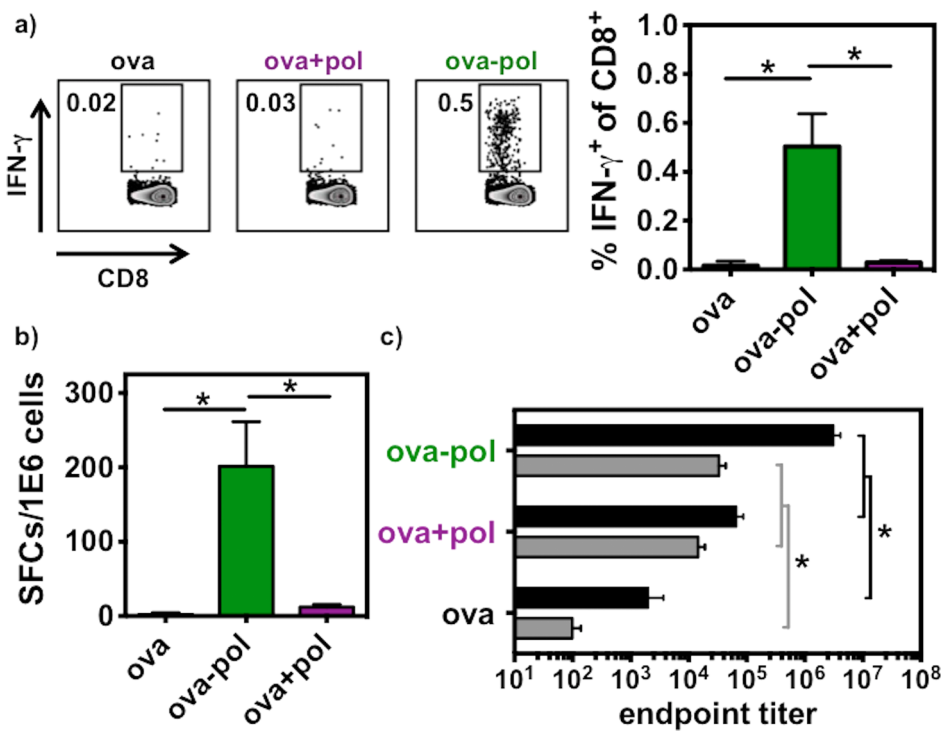


**Figure 5. Immunization with ovalbumin–nanoparticle conjugates enhances CD8 $^{+}$ IFN- $\gamma$  $^{+}$  T cell and antibody responses.** Mice were immunized on days 0 and 21 with free ovalbumin (ova), a physical mixture of ova and micelles (ova+pol), or conjugates (ova-pol) and the immune response characterized on day 28. Splenocytes were restimulated *ex vivo* with ova<sub>257–264</sub> (SIINFEKL) and IFN- $\gamma$  production detected *via* intracellular cytokine staining and ELISPOT. (a) Representative flow cytometry dot plots of CD8 $^{+}$ IFN- $\gamma$  $^{+}$  T cells from individual mice (left) and the average response from groups (right). (b) ELISPOT quantification (SFCs: spot forming cells) of CD8 $^{+}$ IFN- $\gamma$  $^{+}$  T cell response. (c) IgG1 (black bars) and IgG2c (gray bars) antibody end point titers were measured by ELISA from serum collected at day 27. Data represent the mean  $\pm$  SEM of two independent experiments with  $n = 10$  total, with the exception of ova where  $n = 6$ ; \* $p < 0.05$  by ANOVA with Tukey's post-hoc test.

mixture and conjugate might be explained by overall enhancements in antigen uptake with the latter. Vaccination with the conjugate, as well as the mixture, elicited a significantly higher IgG1 than IgG2 titer (IgG2c/IgG1 < 1.0; Figure S4a, Supporting Information), indicating a Th2 bias in the CD4 $^{+}$  response<sup>48</sup> and suggesting a potential adjuvant effect inherent to the nanoparticle. Indeed, a number of polymeric materials, including synthetic polycations, have been shown to possess inherent inflammatory or adjuvant properties<sup>13,49–52</sup> that here may be augmenting Th2 CD4 $^{+}$  T cell and B cell responses without inducing a CD8 $^{+}$  T cell response. Additionally, it is conceivable that the endosomolytic nature of these carriers may have adjuvant effects mediated by the induction of inflammasomes that can induce cytokine production and enhance DC activation.<sup>52</sup>

**Dual-Delivery of Antigen and CpG ODN Enhances CD8 $^{+}$  and Th1 CD4 $^{+}$  Responses *in Vivo*.** Generation of robust CD8 $^{+}$  T cell responses requires not only class I antigen presentation but also additional immunostimulatory signals delivered by antigen-presenting cells and type 1 CD4 $^{+}$  T helper (Th1) cells. A growing class of molecular adjuvants has been developed to stimulate inflammatory pathways that promote Th1-biased responses.<sup>7,53,54</sup> Class B CpG ODNs are a promising type of oligonucleotide adjuvant that are widely investigated clinically.<sup>55,56</sup>

Therefore, we postulated that combining the CTL-inducing capabilities of pH-responsive nanocarriers with the immunopotentiating properties of a class B CpG ODN would allow the benefits of each to be harnessed in a cooperative manner. To test this hypothesis, mice were immunized as described previously with dual-delivery vehicles assembled through electrostatic complexation of CpG ODN 1826, a murine B-type CpG ODN, to nanoparticle–ova conjugates (ova-pol/CpG). To elucidate the importance of delivering both antigen and adjuvant on a common nanoparticle, free ova was mixed with nanoparticles carrying CpG (ova+pol/CpG). Free ova mixed with soluble CpG (ova+CpG) served as an additional control, representing the most common delivery modality for CpG as a vaccine adjuvant. As shown in Figure 6, immunization with dual-delivery nanocarriers dramatically enhanced both CD8 $^{+}$  T cell and Th1 responses relative to those elicited by conjugates (ova-pol), ova administered with free CpG (ova+CpG), or a formulation containing free ova and CpG complexed to polymer (ova+pol/CpG). Dual-delivery of CpG and ova on pH-responsive nanoparticles (ova-pol/CpG) resulted in an average of 3.4% CD8 $^{+}$  T cells (%IFN- $\gamma$  $^{+}$  of CD8 $^{+}$ ) as measured by intracellular cytokine staining (Figure 6a), a  $\sim$ 7-fold increase over the conjugate alone (0.5%) and an  $\sim$ 18-fold increase over antigen administered with free

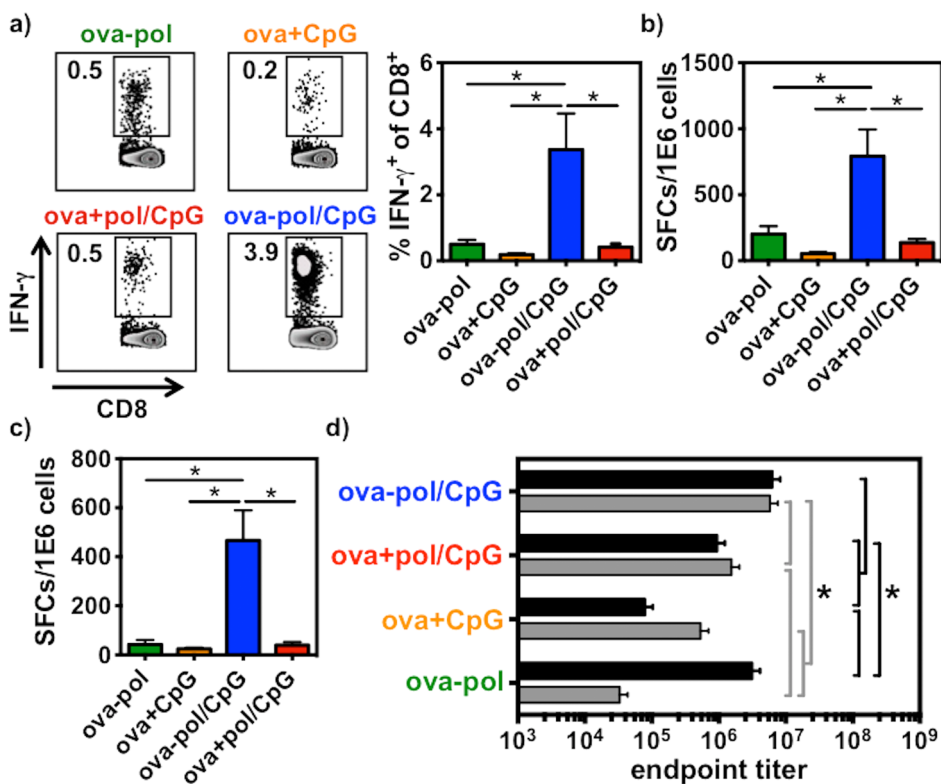


**Figure 6. Dual-delivery of ovalbumin and CpG ODN on pH-responsive nanocarriers enhances CD8<sup>+</sup> T cell and CD4<sup>+</sup> Th1 responses.** Mice were immunized with conjugates (ova-pol), ova mixed with free CpG (ova+CpG), dual-delivery vehicles (ova-pol/CpG), and free ova mixed with CpG/micelle complexes (ova+pol/CpG). Splenocytes were restimulated *ex vivo* with ova<sub>257–264</sub> (SIINFEKL; CD8<sup>+</sup> response) or ova<sub>323–339</sub> (ISQAVHAAHAEAGR; CD4<sup>+</sup> response) and IFN- $\gamma$  production detected via intracellular cytokine staining and ELISPOT. (a) Representative flow cytometry dot plots of CD8<sup>+</sup>IFN- $\gamma$ <sup>+</sup> T cells from individual mice and average response from groups. (b) ELISPOT quantification (SFCs: spot forming cells) of CD8<sup>+</sup>IFN- $\gamma$ <sup>+</sup> T cell response. (c) ELISPOT quantification of CD4<sup>+</sup>IFN- $\gamma$ <sup>+</sup> T cell response. (d) IgG1 (black bars) and IgG2c (gray bars) antibody end point titers were measured by ELISA from serum collected at day 27. Data represent the mean  $\pm$  SEM of two independent experiments with  $n = 10$ ; \* $p < 0.05$  by ANOVA with Tukey's post-hoc test.

CpG (0.18%). Notably, the CD8<sup>+</sup> T cell response elicited by ova–nanoparticle conjugates (ova-pol; 0.5%) was comparable to that induced using soluble CpG ODN 1826 as an adjuvant (0.18%; Figure 6a), providing a metric for the relative capability of these polymeric nanoparticles to enhance CD8<sup>+</sup> T cell responses. Additionally, administration of free ova mixed with CpG/polymer complexes (ova+pol/CpG) did not significantly increase the CD8<sup>+</sup> T cell response relative to free CpG (0.4% vs 0.18%). Similar trends were observed when measuring CD8<sup>+</sup> T cell responses using IFN- $\gamma$  ELISPOT (Figure 6b).

Dual-delivery of antigen and CpG (ova-pol/CpG) also significantly enhanced the Th1 (CD4<sup>+</sup>INF- $\gamma$ <sup>+</sup>) response relative to other experimental groups, all of which elicited comparably low responses as measured by ELISPOT (Figure 6c). Th1 responses were increased  $\sim$ 11-fold relative to the conjugate (ova-pol) and ova mixed with polymer-complexed CpG (ova+pol/CpG) and nearly 20-fold relative to soluble antigen mixed with CpG (ova+CpG). Consistent with the heightened Th1 response, complexation of CpG to nanoparticle–ova conjugates (ova-pol/CpG) increased IgG2c titer nearly 200-fold without significant change in the

IgG1 titer, yielding an IgG2c/IgG1 ratio close to unity (Figure 6d and Figure S4b, Supporting Information), which suggests a balanced Th1/Th2 response. These findings are consistent with several previous reports demonstrating enhanced CpG activity achieved by delivery with antigen on the same vehicle.<sup>20,21,57,58</sup> Significantly, the CD8<sup>+</sup> T cell and Th1 responses elicited with dual-delivery carriers are substantially greater than the additive effects of polymeric antigen conjugation and addition of CpG as an adjuvant.

The ability of dual-delivery carriers to elicit CD8<sup>+</sup> and CD4<sup>+</sup> T cell responses suggests that antigen is accessible to both MHC-I and MHC-II processing pathways, the latter of which may be mediated by a cohort of antigen that remains in endo/lysosomal compartments. A similar response has been observed for antigen encapsulated in virosomes that fail to escape the endosome.<sup>6</sup> Though we employed a pH-responsive tercopolymer with strong endosomolytic activity,<sup>26</sup> the persistence of a CD4<sup>+</sup> response that can act to modulate both cellular and humoral immunity is also an important element of this design. Similarly, these data suggest that CpG complexed with endosomolytic carriers maintains a capacity to engage TLR9 localized in

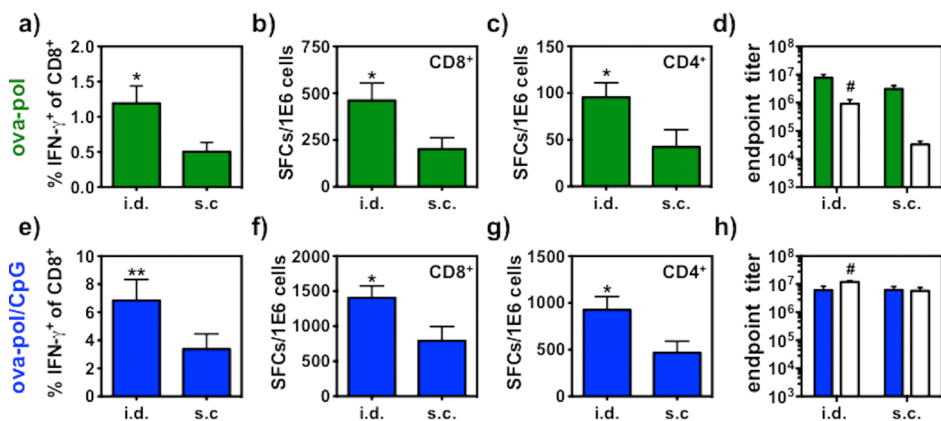


**Figure 7.** Intradermal (i.d.) immunization increases cellular and humoral immune responses relative to subcutaneous (s.c.) administration. CD8<sup>+</sup> T cell response to (a,b) conjugates (ova-pol) and (e,f) dual-delivery vehicles (ova-pol/CpG) determined by intracellular cytokine staining (a,e) and ELISPOT (b,f). Th1 response to conjugates (c) and dual-delivery vehicles (g) measured by ELISPOT. IgG1 (filled bars) and IgG2c (hollow bars) antibody end point titers elicited by conjugates (ova-pol) (d) and dual-delivery (ova-pol/CpG) carriers (h) measured by ELISA. Data represent the mean  $\pm$  SEM of 2–3 independent experiments with  $n = 10$ –16 total; \*\* $p = 0.08$ , \* $p < 0.05$  by student's  $t$  test; # $p < 0.05$ , IgG2c intradermal vs subcutaneous administration by student's  $t$  test.

endosomal compartments. A similar phenomenon has been described for CpG encapsulated in pH-responsive liposomes.<sup>19</sup> Interestingly, this is not the case for all cationic CpG delivery platforms, as a number of cationic carriers have been shown to reduce the adjuvant activity of CpG.<sup>49,59</sup> This may be attributed to the relative accessibility of electrostatically bound CpG in endosomal compartments, which is thought to be influenced by the strength of binding between the polymer and CpG.<sup>59–61</sup> Additionally, particulate carriers can also influence endosomal trafficking, which has been shown to affect the magnitude and nature of the response to CpG.<sup>60,61</sup> For example, complexation of CpG-B with the cationic liposome DOTAP shifted the localization of CpG-B from lysosomes to endosomes, a change that stimulated the production of interferon- $\alpha$  in plasmacytoid DCs.<sup>61</sup> Alternatively, ova or CpG delivered to the cytosol might subsequently be trafficked back to endo/lysosomal compartments through autophagy, the catabolic process that leads to engulfment of cytosol and organelles in autophagic vacuoles that fuse with lysosomes. Indeed, there is considerable evidence that autophagy promotes MHC class II presentation of endogenous cytosolic proteins and proteins of viral origin,<sup>62–64</sup> and therefore, it is conceivable that a cohort of cytosolic ova becomes engulfed in autophagosomes and ultimately is processed for class II presentation. Similarly, Lee *et al.* found that cytosolic RNA intermediates from certain single-stranded RNA viruses must be transported into lysosomes *via* autophagy in order to be recognized by TLR7, another endo/lysosomal TLR;<sup>65</sup> a similar role for autophagy has been postulated in TLR9 recognition of cytosolic CpG-containing DNA.<sup>66</sup> While the effect of polymeric CpG delivery on TLR9 signaling remains to be investigated, these studies suggest that endosomal releasing activity and endosomal signaling are not mutually exclusive events.

#### Intradermal Immunization Further Augments Responses.

Intradermal administration of vaccines offers a potential strategy for enhancing immune responses by improving delivery to antigen-presenting cells abundant in the dermis<sup>67,68</sup> as well as increasing access to lymphatic vessels and lymph nodes.<sup>69</sup> We evaluated responses elicited by both nanoparticle–ova conjugates (ova-pol) and dual-delivery carriers (ova-pol/CpG) that were injected intradermally in the pinna of the ear using the same doses and immunization regimen utilized for subcutaneous administration. Intradermal vaccination enhanced both CD8<sup>+</sup> T cell and Th1 responses approximately 2-fold for both the conjugates (Figure 7a–c) and dual-delivery vehicles (Figure 7e–g). Notably, intradermal vaccination with nanocarriers for dual-delivery of antigen and CpG resulted in an average of 6.8% antigen-specific CD8<sup>+</sup> T cells with responses as high as ~15% percent observed in 2 of 11 mice. Though differences in dose, adjuvant choice, immunization regimen, and characterization techniques render direct comparison difficult, these CD8<sup>+</sup> T cell responses are among the strongest elicited for a protein antigen using a sub-100 nm nanoparticle vaccine.<sup>12,19,70–72</sup> Additionally, intradermal vaccination elicited significantly higher IgG2c titer compared to subcutaneous administration for both conjugates (~30-fold) and dual-delivery carriers (2-fold), while IgG1 titer was not significantly increased, commensurate with the elevated Th1 response (Figure 7d,h). These data demonstrate the capacity of this system to elicit strong cellular and humoral immune responses that may be further enhanced through optimized immunization regimens.

#### CONCLUSION

Through dual-delivery of protein antigen and CpG ODN on endosomolytic nanoparticles, we have developed a

new class of subunit vaccine combining multiple pathogen-inspired cues into a single synthetic platform that actively promotes antigen cross-presentation and stimulates innate immunity. Owing to their pH-dependent membrane destabilizing activity, carriers increased MHC class I antigen presentation with attendant augmentation of antigen-specific CD8<sup>+</sup> T cell responses. Significantly, dual-delivery of antigen and CpG ODN on a single carrier synergistically enhanced both CD8<sup>+</sup> T cell and CD4<sup>+</sup> Th1 T cell responses while eliciting a balanced IgG1/IgG2c antibody response. Though a model antigen was used and immunization regimens remain to be optimized, the considerable magnitude of immune responses elicited

by this vaccine formulation, particularly the CD8<sup>+</sup> T cell response, warrants future evaluation of this technology for vaccination against refractory infectious diseases as well as for the treatment of cancer. Additionally, this modular vaccine delivery platform is composed entirely of synthetic components that can be economically and scalably synthesized and is anticipated to allow for conjugation of diverse antigens and complexation of additional immunomodulatory oligonucleotides. Collectively, these investigations demonstrate the potential of pH-responsive nanoparticles as a multimodal and tunable platform for improving the efficacy of protein subunit vaccines.

## MATERIALS AND METHODS

**Synthesis of Pyridyl Disulfide Ethyl Methacrylate (PDSEMA).** The PDSEMA monomer was synthesized as described previously with minor modifications.<sup>73</sup> Hydroxyethyl pyridyl disulfide (HDPS) was synthesized as described elsewhere.<sup>74</sup> In brief, a total of 3 g (38.5 mmol) of 2-mercaptoethanol was dissolved in MeOH (20 mL) followed by 5 mL of 2,2'-dipyridyl disulfide (10.3 g, 46.2 mmol, Sigma-Aldrich) in MeOH. The reaction mixture was stirred at room temperature under N<sub>2</sub> overnight. MeOH was removed via evaporation and used for the next reaction without further purification (TLC: *R*<sub>f</sub> = 0.4, *R*<sub>f</sub> = 0.8 is the excess 2,2'-dipyridyl disulfide, and *R*<sub>f</sub> = 0.1 is 2-pyridinethione). Then, a total of 4 g (21.4 mmol) of HDPS was placed in a dry round-bottom flask followed by 50 mL of anhydrous dichloromethane (DCM). The solution was cooled using an ice bath for another 5 min, and a total of 3.58 mL of TEA (25.7 mmol) was subsequently added to the reaction mixture. Finally, methacryloyl chloride (3.1 mL, 32.0 mmol, Sigma-Aldrich) in 10 mL of DCM was added dropwise to the precooled reaction mixture while stirring under nitrogen. The reaction was stirred in an ice bath for an additional 2 h and transferred to room temperature overnight. Formation of PDSEMA monomer was monitored by TLC using 33:67 ethyl acetate/hexane solvent mixture as the mobile phase (*R*<sub>f</sub> = 0.55, other impurities all below *R*<sub>f</sub> = 0.35). The reaction mixture was diluted with DCM and subsequently washed with brine. The collected organic phase was dried by anhydrous MgSO<sub>4</sub> and the organic solvent removed *in vacuo*. The crude product was further purified via column chromatography using ethyl acetate/hexane as the mobile phase (packing with pure hexane and increasing EA from 20 to 40%). <sup>1</sup>H NMR (CDCl<sub>3</sub>): δ 1.9 (3H, m), 3.1 (2H, t), 4.4 (2H, t), 5.6 (1H, m), 6.1 (1H, m), 7.1 (1H, m), 7.6 (1H, m), 7.7 (1H, m), 8.5 (1H, m).

**RAFT Polymerization of Poly[(DMAEMA-*co*-PDSEMA]-block-(DMAEMA-*co*-BMA-*co*-PAA)].** RAFT copolymerization of dimethylaminoethyl methacrylate (DMAEMA) and PDSEMA was conducted under a nitrogen atmosphere in dioxane (40 wt % monomer) at 30 °C for 18 h with 4-cyano-4-(ethylsulfanylthiocarbonyl)sulfanylpentanoic acid (ECT)<sup>26</sup> and 2,2'-azobis(4-methoxy-2,4-dimethyl valeronitrile) (V-70) (Wako Chemicals) as the RAFT chain transfer agent and initiator, respectively. All monomers were distilled prior to use. The initial molar ratio of DMAEMA to PDSEMA was 95:5, and the initial monomer ([M]<sub>0</sub>) to CTA ([CTA]<sub>0</sub>) to initiator ([I]<sub>0</sub>) ratio was 100:1:0.05. The resultant poly(DMAEMA-*co*-PDSEMA) macro-chain transfer agent (mCTA) was isolated by precipitation (6×) into pentane. The mCTA was dried for 1 week *in vacuo* and subsequently used for block copolymerization of DMAEMA, propylacrylic acid (PAA), and butyl methacrylate (BMA), as previously described with minor modifications.<sup>27</sup> DMAEMA (30%), PAA (30%), and BMA (40%) ([M]<sub>0</sub>/[CTA]<sub>0</sub> = 450) were added to the mCTA dissolved in dimethylacetamide (40 wt % monomer and mCTA) along with the free radical initiator V-70 at a mCTA to initiator ratio ([mCTA]<sub>0</sub>/[I]<sub>0</sub>) of 2.5. The polymerization was allowed to proceed under a nitrogen atmosphere for 24 h at 30 °C. The resultant diblock copolymer was

isolated by initial precipitation into 80:20 pentane/ether and subsequently redissolved in acetone and precipitated (6×) into pentane. The product was then dried *in vacuo* for 48 h, reconstituted into molecular grade water (HyClone) from a stock solution prepared in ethanol, and subsequently lyophilized for 96 h. The composition of both the mCTA and diblock copolymer was analyzed by <sup>1</sup>H NMR (CDCl<sub>3</sub>) spectroscopy (Bruker AV 500). Gel permeation chromatography (GPC) was used to determine molecular weights and polydispersities (*M*<sub>w</sub>/*M*<sub>n</sub>, PDI) of both the mCTA and diblock copolymer. SEC Tosoh TSK-GEL R-3000 and R-4000 columns (Tosoh Bioscience, Montgomeryville, PA) were connected in series to a Agilent 1200 series (Agilent Technologies, Santa Clara, CA), refractometer Optilab-rEX, and a triple-angle static light scattering detector miniDAWN TREOS (Wyatt Technology, Santa Barbara, CA). HPLC-grade DMF containing 0.1 wt % LiBr at 60 °C was used as the mobile phase at a flow rate of 1 mL/min. The molecular weights of each polymer were determined using a multidecetector calibration based on *d*<sub>n</sub>/*d*<sub>c</sub> values calculated separately for each copolymer (0.071 and 0.065 for mCTA and diblock, respectively). Additionally, the number of pyridyl disulfide groups per polymer chain was determined to be 1.5 based on spectrophotometric determination of the amount of pyridine-2-thione released (343 nm,  $\epsilon$  = 8080 M<sup>-1</sup> cm<sup>-1</sup>) after incubation with 5 mM TCEP (Bond-Breaker TCEP, Thermo Scientific) for 1 h. Additional synthetic details, representative NMR spectra, and a summary of polymer properties can be found in the Supporting Information.

**Formulation of Polymer Micelles.** Aqueous polymer solutions were prepared by first dissolving the dry copolymer into ethanol at 50 mg/mL followed by rapid dilution into sodium phosphate buffer (100 mM, pH 7.0) to a final concentration of 10 mg/mL. Ethanol was removed by buffer exchange into phosphate buffered saline (PBS; 137 mM NaCl, 2.7 mM KCl, 8 mM Na<sub>2</sub>HPO<sub>4</sub>, 2 mM KH<sub>2</sub>PO<sub>4</sub>; Ambion) via four cycles of centrifugal dialysis (Amicon, 3 kDa MWCO, Millipore). In selected instances, the ethanol content of the final polymer solution was determined via the Amplete ethanol quantitation kit (AAT Bioquest) according to manufacturer's instructions and consistently found to be below 0.1%. Polymers were sterilized prior to use via 0.22  $\mu$ m syringe filtration (Pall Corporation). Polymer concentration was determined spectrophotometrically via absorbance of the aromatic PDS groups at 284 nm.

**Preparation of Polymer-Ovalbumin Conjugates.** Ovalbumin (ova) was conjugated to PDS groups on polymer micelles via a disulfide exchange reaction. Thiol groups were incorporated onto ova using a 22 molar excess of 2-iminothiolane (Traut's reagent) as previously described.<sup>25</sup> Nonreacted 2-iminothiolane was removed using a Zeba desalting column (0.5 mL, 7 K MWCO; Thermo Scientific) equilibrated with 1× PBS (pH 7.4). The solution was then sterile-filtered and the average number of thiol groups per ova determined using Ellman's reagent (Thermo Scientific) according to manufacturer instructions. For all studies, 3–5 thiols per ova were introduced. In some instances, ova was labeled with AlexaFluor488-TFP (Invitrogen)

prior to thiolation with  $\sim$ 0.5–1 dye/protein according to manufacturer instructions. Thiolated ova was subsequently reacted with polymer micelles (prepared as described above) at a 20:1 polymer/ova molar ratio in PBS under sterile conditions. The extent of conjugation was determined *via* nonreducing SDS-polyacrylamide gel electrophoresis (SDS-PAGE) of conjugates prepared with fluorescently labeled ova (137 V; 4–20% Tris-glycine; PROTEAN TGC precast gel, Bio-Rad). To demonstrate the reducibility of the disulfide bond between polymer and protein, conjugates were incubated with 10 mM glutathione (Sigma-Aldrich) for 1 h at room temperature. Gels were imaged using a Storm 860 Molecular Imager (GMI Inc.) to determine protein shifts and ImageQuant TL software was used to quantify the extent of conjugation.

**Formation of Polymer/CpG Complexes.** Polymer/CpG complexes were formed by combining CpG ODN 1826 (Invivogen) and micelle solution in PBS for 30 min at room temperature at different theoretical charge ratios. The charge ratio was defined as the molar ratio between protonated DMAEMA tertiary amines in the first block (assuming 50% protonation at physiological pH) and phosphate groups along the CpG backbone. The charge ratio at which polymers mediated complete CpG complexation was determined *via* an agarose gel retardation assay. Free CpG and complexes prepared at various charge ratios were loaded into lanes of a 4% agarose gel and run at 90 V for 1 h. Gels were stained with SYBR Safe (Invitrogen) for 1 h and subsequently visualized with a Storm 860 Molecular Imager (GMI).

**Static and Dynamic Light Scattering.** Static light scattering measurements were performed on a Nanoseries Zetasizer (Malvern) at a constant scattering angle of 173°. The micelle molecular weight ( $M_w$ ) and second virial coefficient ( $A_2$ ) were estimated from the relationship:  $KC_p/R_0 = 1/M_w + 2A_2C_p$ , where  $K$ ,  $C_p$ ,  $M_w$ ,  $R_0$ , and  $A_2$  are the optical constant, polymer concentration, molecular weight, Rayleigh ratio, and second virial coefficient, respectively. The  $d\ln/dc$  of the micelle solution was measured using an Optilab-REX refractometer (Wyatt Technology, Santa Barbara, CA) and determined to be 0.161. By measuring  $R_0$  at a series of  $C_p$  values between 0.75 and 0.15 mg/mL,  $M_w$  and  $A_2$  were estimated from Debye plots. Micelle aggregation number ( $N_{agg}$ ) was determined by comparing the molecular weight of the diblock copolymer micelles ( $M_w$ ) to the molecular weight of the unimeric species as determined by GPC using the relation  $N_{agg} = M_w/\text{micelle}/M_w/\text{unimer}$ . The sizes of free diblock copolymer micelles, micelle–ova conjugates, and conjugate/CpG complexes were determined by dynamic light scattering (DLS) using a Nanoseries Zetasizer (Malvern) at a constant scattering angle of 173°. All samples were analyzed at room temperature in PBS (pH 7.4) normalized to 0.1 mg/mL polymer. Mean diameters are reported as the number average  $\pm$  standard deviation from a minimum of three independently prepared formulations.

**Cell Lines.** The mouse dendritic cell line DC2.4 (H-2K<sup>b</sup>-positive) was kindly provided by K. Rock (University of Massachusetts Medical School) and cultured in RPMI 1640 (Gibco) supplemented with 10% fetal bovine serum (FBS; Gibco), 2 mM L-glutamine, 100 U/mL penicillin/100 µg/mL streptomycin (Gibco), 55 µM 2-mercaptoethanol (Gibco), 1× nonessential amino acids (Cellgro), and 10 mM HEPES (Invitrogen). B3Z T cells, a lacZ-inducible T cell hybridoma specific for the SIINFEKL-H-2K<sup>b</sup> complex, were a generous gift from Nilabh Shastri (UC Berkeley) and cultured in RPMI 1640 (Gibco) supplemented with 10% FBS, 100 U/mL penicillin/100 µg/mL streptomycin (Cellgro), 50 µM 2-mercaptoethanol (Gibco), and 1 mM sodium pyruvate (Gibco). Both cell types were grown in a humidified atmosphere with 5% CO<sub>2</sub> at 37 °C.

**In Vitro Cross-Presentation Assay.** The ability of polymeric nanoparticles to enhance MHC class I antigen presentation was assessed by an *in vitro* antigen presentation assay<sup>19,24,75</sup> using DC2.4 cells<sup>39</sup> as the antigen-presenting cell. This assay utilizes a specialized LacZ B3Z T cell hybridoma that produces β-galactosidase upon recognition of the immunodominant ovalbumin class I epitope SIINFEKL presented on MHC class I H-2K<sup>b</sup> on DC2.4 cells.<sup>76</sup> DC2.4 cells were plated at  $5 \times 10^4$  cells/well in U-bottom 96-well cell culture plates and grown overnight. The following day, ova–nanoparticle conjugates and controls were added to a final concentration of 1 µg/mL ova and incubated with DC2.4 cells for 4 h at 37 °C in a 5% CO<sub>2</sub> incubator. Cells were

then carefully rinsed 3× with DPBS, and  $10 \times 10^4$  B3Z T cells were added to each well and cocultured for 22–24 h in RPMI 1640 supplemented with 10% FBS, 2 mM L-glutamine, 55 µM β-mercaptoethanol, 1 mM pyruvate, and 100 U/mL penicillin/100 µg/mL streptomycin. Cells were then pelleted *via* centrifugation (7 min,  $\sim$ 500 rcf), media carefully aspirated, and 150 µL of CPRG/lysis buffer (0.15 mM chlorophenol red-β-D-galactopyranoside (CalBiochem), 0.1% Triton-X 100, 9 mM MgCl<sub>2</sub>, 100 µM mercaptoethanol) added. Plates were incubated at 37 °C in the dark for 90 min, and the absorbance of released chlorophenol red was measured at 570 nm using a Tecan Safire 2 plate reader.

To elucidate the intracellular processing pathways associated with polymer-mediated cross-presentation, DC2.4 cells were incubated with conjugates or controls in the presence or absence of 100 µM chloroquine, an inhibitor of endosomal acidification,<sup>77</sup> the proteasome inhibitor lactacystin (3 µM),<sup>78</sup> or brefeldin A (GolgiPlug, BD), an inhibitor of TAP-mediated translocation of MHC-I molecules to the cell surface.<sup>77</sup> Conjugates and controls were added to cells 1 h after addition of inhibitors. After 4 h, cells were washed 3× with DPBS, fixed on ice for 5 min with 1% paraformaldehyde, and washed again 3× with DPBS<sup>79</sup> prior to addition of  $50 \times 10^3$  B3Z cells as described above. In a parallel study, cell viability was determined after incubation with conjugates and inhibitors using an MTS cell viability assay (Promega). Chlorophenol red absorbance (570 nm) data were normalized to viability to account for small differences in cell viability induced by treatment with inhibitors; in all instances, cell viability after treatment with conjugates and inhibitors was determined to be greater than 70% of untreated control.

**Erythrocyte Lysis Assay.** The capacity of free polymer, ova–polymer conjugates, and conjugate/CpG complexes to induce pH-dependent disruption of lipid bilayer membranes was assessed *via* a red blood cell hemolysis assay as previously described.<sup>80</sup> Briefly, polymers were incubated for 1 h at 37 °C in the presence of human erythrocytes at 2.5 µg/mL in 100 mM sodium phosphate buffer (supplemented with 150 mM NaCl) in the pH range of the endosomal processing pathway (7.4, 7.0, 6.6, 6.2, and 5.8). Extent of cell lysis (*i.e.*, hemolytic activity) was determined spectrophotometrically by measuring the amount of hemoglobin released (abs = 541 nm) and normalized to a 100% lysis control (1% Triton X-100). Samples were run in quadruplicate.

**In Vitro Dendritic Cell Uptake.** Intracellular uptake of ovalbumin and CpG was evaluated by flow cytometry using AlexaFluor488-labeled ovalbumin and 3'-TAMRA-labeled CpG (Integrated DNA Technologies). DC2.4 cells were plated at 75k cells/well in 24-well plates and allowed to adhere overnight. Cells were subsequently incubated with formulations containing fluorescently labeled ova and CpG for the indicated amount of time, rinsed 2× with DPBS, trypsinized (0.25%, 5 min), pelleted by centrifugation, and resuspended in DPBS containing 2% FBS. Flow cytometry was performed on a FACSCantoll (BD) and analyzed using FlowJo software (Tree Star Inc.). To determine the initial rate of ova and CpG uptake by DC2.4 cells, the median fluorescent intensity (MFI) was plotted as a function of time over a 4 h incubation period, fit with a linear regression, and the initial rate of uptake was defined as the slope of the line. To investigate the mechanism of uptake, cells were preincubated for 30 min at 4 °C or at 37 °C in the presence of chlorpromazine (10 µg/mL), 5-(N,N-dimethyl)amiloride (150 µg/mL),<sup>32</sup> or genistein (50 µg/mL)<sup>81</sup> followed by addition of CpG and/or ova-containing samples for 1 h.

**Animals.** Female C57BL/6 mice, 6–8 weeks old, were obtained from The Jackson Laboratory (Bar Harbor, ME). All animals were maintained at the University of Washington under specific pathogen-free conditions and treated in accordance with the regulations and guidelines of the University of Washington Institutional Animal Care and Use Committee.

**Immunization of Mice.** All vaccine formulations were prepared using a low endotoxin grade ovalbumin (<0.01 EU/g; Endo-Grade; Hyglos GmbH), and sterile, endotoxin-, protease-, and nuclease-free water (Invivogen) and PBS (Ambion). To confirm low endotoxin content of vaccines, formulations were periodically assayed for endotoxin content using a Limulus amoebocyte lysate assay kit (Lonza) and consistently found to be less than 5 EU/kg as recommended by the United States Pharmacopoeia.<sup>82</sup> Groups of mice ( $n = 6$ –16 per group) were immunized

subcutaneously at the base of the tail or intradermally in the pinna of the ear with formulations containing 25  $\mu$ g ova with or without 28  $\mu$ g of CpG and/or 360  $\mu$ g polymer in PBS. Mice were immunized at days 0 and 21 in opposite sides (s.c.) or ears (i.d.) using a 0.3 cc syringe with a 30 gauge needle. Subcutaneous and intradermal immunizations were delivered in 200 and 20  $\mu$ L, respectively, and intradermal injections were performed under isoflurane anesthesia. Experimental groups were as follows: free ovalbumin (ova), a physical mixture of micelles and ova (ova+pol), nanoparticle–ova conjugate (ova-pol), ova mixed with free CpG (ova+CpG), CpG complexed with nanoparticle–ova conjugates (ova-pol/CpG), and free ova combined with CpG complexed to polymeric carriers (ova+pol/CpG). Conjugates were prepared 18–24 h prior to immunization and all other formulations prepared within 3 h of injection. Animals were monitored for weight loss and signs of lethargy, and no adverse effects were observed with any formulation tested.

**Preparation of Splenocyte Culture.** One week post boost immunization (day 28), mice were sacrificed and spleens harvested for preparation of splenocyte cultures. Individual spleens were mechanically digested into single-cell suspensions in complete RPMI 1640 media (cRPMI; 10% FCS, 100 U/mL penicillin, 100  $\mu$ g/mL streptomycin, 50  $\mu$ M 2-mercaptoethanol, and 2 mM L-glutamine) by forcing them through a 100  $\mu$ m cell strainer (BD) using a sterile syringe plunger. The cell suspension was subsequently filtered through a 70  $\mu$ m cell strainer to remove any residual tissue fragments, and erythrocytes were removed by treatment with ammonium chloride (PharmLyse, BD). Cells were then washed twice and resuspended in cRPMI.

**Intracellular Cytokine Staining.** Splenocytes were plated in 96-well U-bottom plates at  $2 \times 10^6$  cells/well in cRPMI and cultured in the presence or absence of 20  $\mu$ g/mL of the class I epitope ova<sub>257–264</sub> (SIINFEKL) at 37 °C and 5% CO<sub>2</sub>. After 1 h, a protein transport inhibitor (GolgiPlug; BD Bioscience) was added to each well for an additional 8 h. After incubation, cells were washed with PBS supplemented with 2% FBS (Stain Buffer; BD Bioscience), incubated with Fc-block (anti-CD16/CD32; BD Bioscience) for 15 min at 4 °C, washed again, and subsequently stained with AlexaFluor488-conjugated rat anti-mouse CD8a antibody for 30 min at 4 °C (BD Bioscience). Following an additional wash, cells were fixed and permeabilized for 20 min at 4 °C with BD Cytofix/Cytoperm (BD Bioscience) according to manufacturer instructions. Cells were then washed 2× with perm/wash buffer (BD Bioscience) and incubated for 30 min at 4 °C with APC-conjugated rat anti-mouse IFN- $\gamma$  antibody (BD Bioscience) in permeabilization buffer. Following 3× wash with perm/wash buffer, cells were resuspended in stain buffer and analyzed by flow cytometry using a FACSCantoll flow cytometer (BD) and FlowJo software (Tree Star, Inc.). Splenocytes viable at the time of fixation were gated by forward and side scatter, height, and width, and a minimum of 100 000 events within this population were acquired for each sample. Data are reported as the percentage of CD8<sup>+</sup> cells that are IFN- $\gamma$ <sup>+</sup> (i.e., INF- $\gamma$ <sup>+</sup> of CD8<sup>+</sup>) after subtraction of background values from unstimulated controls. Data are pooled from 2 to 3 independent experiments.

**Enzyme-Linked Immunosorbent Spot Assay (ELISPOT).** Splenocytes from each mouse were evaluated for antigen-specific IFN- $\gamma$  production by ELISPOT (Ready-Set-Go! Mouse IFN- $\gamma$  ELISPOT kit; eBioscience) according to manufacturer's instructions with minor modifications. 96-Well nitrocellulose MultiScreen filter plates (Millipore) were treated briefly with 15  $\mu$ L of 35% ethanol in water, washed 3× with coating buffer, and coated overnight at 4 °C with anti-mouse IFN- $\gamma$  monoclonal antibody at the recommended dilution. The following day, plates were washed 3× with coating buffer and blocked with 200  $\mu$ L of cRPMI for 2 h at 37 °C. Medium was aspirated and the appropriate stimulant or control added: 20  $\mu$ g/mL ova<sub>257–264</sub> (CD8<sup>+</sup>), 20  $\mu$ g/mL ova<sub>323–339</sub> (ISQAVHAAHAEINEAGR; CD4<sup>+</sup>), 3  $\mu$ g/mL concanavalin A (positive control), and cRPMI (negative control). Immediately thereafter, splenocytes were plated in quadruplicate at 1.5 or  $3 \times 10^5$  cells/well and incubated for 36 h at 37 °C. Plates were subsequently washed twice with molecular-grade water (HyClone) followed by three washes with wash buffer (0.05% Tween/PBS) and incubated for 2 h at room temperature with

biotin-conjugated rat anti-mouse IFN- $\gamma$  detection antibody. Plates were washed four times with wash buffer and incubated with avidin-HRP for 45 min at room temperature. Following three washes with wash buffer and two washes with PBS, 100  $\mu$ L of AEC peroxidase substrate (Vector Laboratories), prepared according to manufacturer instructions, was added to each well and left to develop for 20 min. Plates were then washed 5× with water, dried overnight, and the number of spots counted using an ImmunoSpot ELISPOT reader and analysis software package (Cellular Technology Limited). The average number of spots counted upon peptide stimulation was subtracted from the number of spots counted upon incubation with cRPMI (i.e., background), and data are reported as the number of spot forming cells (SFCs) normalized to  $1 \times 10^6$  cells. Data are pooled from 2 to 3 independent experiments.

**Antibody Titer.** Approximately 100  $\mu$ L of blood was collected from mice via submandibular bleeding 1 day before sacrifice (day 27), and sera were tested for ova-specific IgG1 and IgG2c. Nunc MaxiSorp plates (Nunc-Thermo Fisher Scientific Inc.) were coated with 5  $\mu$ g/mL ovalbumin in 1× PBS overnight at 4 °C. Plates were blocked with Super Block blocking buffer (Thermo Scientific) for 15 min followed by five washes with PBS-Tween 20 (PBST). After repeating the blocking step, sera were added at a 1/50 dilution and subsequent 5-fold serial dilutions in 0.1% BSA/PBST and incubated for 2 h at room temperature. Sera from one naïve mouse were run on each plate to determine cutoff values. Post-incubation, plates were washed 5× with PBST and incubated with biotin-conjugated anti-mouse antibodies to IgG1 (BD Pharmingen) or IgG2c (Bethyl Laboratories) at 0.005  $\mu$ g/mL in 0.1% BSA/PBST for 1 h at room temperature. Plates were again washed and incubated with SA-HRP (BD Pharmingen) at a 1:20 000 dilution in 0.1% BSA/PBST for 30 min at room temperature. Following a final round of washes, plates were developed with 100  $\mu$ L SureBlue Reserve TMB 1 peroxidase substrate (KPL). After 5 min, the enzymatic reaction was quenched with 1 M HCl and plates were read within 30 min at 450 nm using a Tecan Safire 2 microplate reader. End point titers were determined from reciprocal dilutions using a sigmoidal fit (GraphPad Prism 5; GraphPad Software Inc.) to determine the dilution at which the 450 nm o.d. value was equal to the mean + two standard deviations of that of naïve serum. Titer values too low for detection were fixed at 100, corresponding to the lowest dilution used here.

**Conflict of Interest:** The authors declare the following competing financial interest(s): Some of the polymeric carriers described in this report have been licensed to PhaseRx Inc. Professor Stayton is a founder of PhaseRx. None of the work described in the report was funded by PhaseRx and the company played no role in any of the research reported.

**Acknowledgment.** The authors would like to thank L. Castelli and J.M. Goverman (University of Washington Department of Immunology) for their assistance with ELISPOT. We would also like to acknowledge M.L. Disis and D. Cecil in the Tumor Vaccine Group at the University of Washington for helpful feedback and insightful scientific discussions related to the manuscript. We are grateful to the National Institutes of Health (R01EB002991 (P.S.S.) and R01AI074661 (C.C., J. Bryers PI)), the Washington State Life Science Discovery Fund (Grant No. 2496490 to the Center for Intracellular Delivery of Biologics), the National Science Foundation IGERT program (DGE-9987620, M.J.M.) and Graduate Research Fellowship under Grants DGE-0718124 (C.C.) and DGE-1256082 (S.K.), the Department of Defense through the National Defense Science and Engineering Graduate Fellowship Program (C.C.), and the Irvington Institute Fellowship Program of the Cancer Research Institute (J.T.W.) for funding this research.

**Supporting Information Available:** Detailed scheme of polymer synthesis, additional polymer characterization data (<sup>1</sup>H NMR and GPC), and additional *in vitro* and *in vivo* data. This material is available free of charge via the Internet at <http://pubs.acs.org>.

## REFERENCES AND NOTES

- Black, M.; Trent, A.; Tirrell, M.; Olive, C. Advances in the Design and Delivery of Peptide Subunit Vaccines with a Focus on Toll-like Receptor Agonists. *Expert Rev. Vaccines* **2010**, 9, 157–173.

2. Perrie, Y.; Mohammed, A. R.; Kirby, D. J.; McNeil, S. E.; Bramwell, V. W. Vaccine Adjuvant Systems: Enhancing the Efficacy of Sub-Unit Protein Antigens. *Int. J. Pharm.* **2008**, *364*, 272–280.
3. Moon, J. J.; Huang, B.; Irvine, D. J. Engineering Nano- and Microparticles To Tune Immunity. *Adv. Mater.* **2012**, *24*, 3724–3746.
4. Ahmed, S. S.; Plotkin, S. A.; Black, S.; Coffman, R. L. Assessing the Safety of Adjuvanted Vaccines. *Sci. Transl. Med.* **2011**, *3*, 93rv2.
5. Hubbell, J. A.; Thomas, S. N.; Swartz, M. A. Materials Engineering for Immunomodulation. *Nature* **2009**, *462*, 449–460.
6. De Temmerman, M.-L.; Rejman, J.; Demeester, J.; Irvine, D. J.; Gander, B.; De Smedt, S. C. Particulate Vaccines: On the Quest for Optimal Delivery and Immune Response. *Drug Discovery Today* **2011**, *16*, 569–582.
7. Foged, C.; Hansen, J.; Agger, E. M. License to Kill: Formulation Requirements for Optimal Priming of CD8(+) CTL Responses with Particulate Vaccine Delivery Systems. *Eur. J. Pharm. Sci.* **2012**, *45*, 482–491.
8. Yewdell, J. W. Designing CD8+ T Cell Vaccines: It's Not Rocket Science (Yet). *Curr. Opin. Immunol.* **2010**, *22*, 402–410.
9. Amigorena, S.; Savina, A. Intracellular Mechanisms of Antigen Cross-Presentation in Dendritic Cells. *Curr. Opin. Immunol.* **2010**, *22*, 109–117.
10. Zhang, N.; Bevan, M. J. CD8(+) T Cells: Foot Soldiers of the Immune System. *Immunity* **2011**, *35*, 161–168.
11. Liu, M. A. Immunology Basis of Vaccine Vectors. *Immunity* **2010**, *33*, 504–515.
12. Moon, J. J.; Suh, H.; Bershteyn, A.; Stephan, M. T.; Liu, H.; Huang, B.; Sohail, M.; Luo, S.; Ho, U. S.; Khant, H.; et al. Interbilayer-Crosslinked Multilamellar Vesicles as Synthetic Vaccines for Potent Humoral and Cellular Immune Responses. *Nat. Mater.* **2011**, *10*, 243–251.
13. Reddy, S. T.; van der Vlies, A. J.; Simeoni, E.; Angeli, V.; Randolph, G. J.; O'Neil, C. P.; Lee, L. K.; Swartz, M. A.; Hubbell, J. A. Exploiting Lymphatic Transport and Complement Activation in Nanoparticle Vaccines. *Nat. Biotechnol.* **2007**, *25*, 1159–1164.
14. Nembrini, C.; Stano, A.; Dane, K. Y.; Ballester, M.; van der Vlies, A. J.; Marsland, B. J.; Swartz, M. A.; Hubbell, J. A. Nanoparticle Conjugation of Antigen Enhances Cytotoxic T-Cell Responses in Pulmonary Vaccination. *Proc. Natl. Acad. Sci. U.S.A.* **2011**, *108*, E989–E997.
15. Kwon, Y. J.; James, E.; Shastri, N.; Fréchet, J. M. J. In Vivo Targeting of Dendritic Cells for Activation of Cellular Immunity Using Vaccine Carriers Based on pH-Responsive Microparticles. *Proc. Natl. Acad. Sci. U.S.A.* **2005**, *102*, 18264–18268.
16. Kasturi, S. P.; Skountzou, I.; Albrecht, R. A.; Koutsonanos, D.; Hua, T.; Nakaya, H. I.; Ravindran, R.; Stewart, S.; Alam, M.; Kwissa, M.; et al. Programming the Magnitude and Persistence of Antibody Responses with Innate Immunity. *Nature* **2011**, *470*, 543–547.
17. Lee, I.-H.; Kwon, H.-K.; An, S.; Kim, D.; Kim, S.; Yu, M. K.; Lee, J.-H.; Lee, T.-S.; Im, S.-H.; Jon, S. Imageable Antigen-Presenting Gold Nanoparticle Vaccines for Effective Cancer Immunotherapy *In Vivo*. *Angew. Chem., Int. Ed.* **2012**, *51*, 8800–8805.
18. Scott, E. A.; Stano, A.; Gillard, M.; Maio-Liu, A. C.; Swartz, M. A.; Hubbell, J. A. Dendritic Cell Activation and T Cell Priming with Adjuvant- and Antigen-Loaded Oxidation-Sensitive Polymericosomes. *Biomaterials* **2012**, *33*, 6211–6219.
19. Andrews, C. D.; Huh, M.-S.; Patton, K.; Higgins, D.; Van Nest, G.; Ott, G.; Lee, K.-D. Encapsulating Immunostimulatory CpG Oligonucleotides in Listeriolysin O-Liposomes Promotes a Th1-Type Response and CTL Activity. *Mol. Pharmaceutics* **2012**, *9*, 1118–1125.
20. Beaudette, T. T.; Bachelder, E. M.; Cohen, J. A.; Obermeyer, A. C.; Broaders, K. E.; Fréchet, J. M. J.; Kang, E.-S.; Mende, I.; Tseng, W. W.; Davidson, M. G.; et al. *In Vivo* Studies on the Effect of Co-encapsulation of CpG DNA and Antigen in Acid-Degradable Microparticle Vaccines. *Mol. Pharmaceutics* **2009**, *6*, 1160–1169.
21. Schlosser, E.; Mueller, M.; Fischer, S.; Basta, S.; Busch, D. H.; Gander, B.; Groettrup, M. TLR Ligands and Antigen Need To Be Coencapsulated Into the Same Biodegradable Microsphere for the Generation of Potent Cytotoxic T Lymphocyte Responses. *Vaccine* **2008**, *26*, 1626–1637.
22. Gruenberg, J.; van der Goot, F. G. Mechanisms of Pathogen Entry through the Endosomal Compartments. *Nat. Rev. Mol. Cell Biol.* **2006**, *7*, 495–504.
23. Cho, Y. W.; Kim, J.-D.; Park, K. Polycation Gene Delivery Systems: Escape from Endosomes to Cytosol. *J. Pharm. Pharmacol.* **2003**, *55*, 721–734.
24. Flanary, S.; Hoffman, A. S.; Stayton, P. S. Antigen Delivery with Poly(propylacrylic acid) Conjugation Enhances MHC-1 Presentation and T-Cell Activation. *Bioconjugate Chem.* **2009**, *20*, 241–248.
25. Foster, S.; Duvall, C. L.; Crownover, E. F.; Hoffman, A. S.; Stayton, P. S. Intracellular Delivery of a Protein Antigen with an Endosomal-Releasing Polymer Enhances CD8 T-Cell Production and Prophylactic Vaccine Efficacy. *Bioconjugate Chem.* **2010**, *21*, 2205–2212.
26. Convertine, A. J.; Benoit, D. S. W.; Duvall, C. L.; Hoffman, A. S.; Stayton, P. S. Development of a Novel Endosomolytic Diblock Copolymer for siRNA Delivery. *J. Controlled Release* **2009**, *133*, 221–229.
27. Convertine, A. J.; Diab, C.; Prieve, M.; Paschal, A.; Hoffman, A. S.; Johnson, P. H.; Stayton, P. S. pH-Responsive Polymeric Micelle Carriers for siRNA Drugs. *Biomacromolecules* **2010**, *11*, 2904–2910.
28. Bode, C.; Zhao, G.; Steinhagen, F.; Kinjo, T.; Klinman, D. M. CpG DNA as a Vaccine Adjuvant. *Expert Rev. Vaccines* **2011**, *10*, 499–511.
29. Krieg, A. M. Therapeutic Potential of Toll-like Receptor 9 Activation. *Nat. Rev. Drug Discovery* **2006**, *5*, 471–484.
30. Szablanski, Z.; Toy, A. A.; Terrenoire, A.; Davis, T. P.; Stenzel, M. H.; Müller, A. H. E.; Barner-Kowollik, C. Living Free-Radical Polymerization of Sterically Hindered Monomers: Improving the Understanding of 1,1-Disubstituted Monomer Systems. *J. Polym. Sci., Part A: Polym. Chem.* **2006**, *44*, 3692–3710.
31. Szablanski, Z.; Toy, A. A.; Davis, T. P.; Hao, X.; Stenzel, M. H.; Barner-Kowollik, C. Reversible Addition Fragmentation Chain Transfer Polymerization of Sterically Hindered Monomers: Toward Well-Defined Rod/Coil Architectures. *J. Polym. Sci., Part A: Polym. Chem.* **2004**, *42*, 2432–2443.
32. Boley, G.; Lassus, A.; Bussat, P.; Terrettaz, J.; Tranquart, F.; Corthésy, B. Gas-Filled Microbubble-Mediated Delivery of Antigen and the Induction of Immune Responses. *Biomaterials* **2012**, *33*, 5935–5946.
33. Fothergill, L. A.; Fothergill, J. E. Thiol and Disulphide Contents of Hen Ovalbumin. C-Terminal Sequence and Location of Disulphide Bond. *Biochem. J.* **1970**, *116*, 555–561.
34. Schafer, F. Q.; Buettner, G. R. Redox Environment of the Cell As Viewed through the Redox State of the Glutathione Disulfide/Glutathione Couple. *Free Radical Biol. Med.* **2001**, *30*, 1191–1212.
35. Hirosue, S.; Kourtis, I. C.; van der Vlies, A. J.; Hubbell, J. A.; Swartz, M. A. Antigen Delivery to Dendritic Cells by Poly(propylene sulfide) Nanoparticles with Disulfide Conjugated Peptides: Cross-Presentation and T Cell Activation. *Vaccine* **2010**, *28*, 7897–7906.
36. Wendorf, J.; Singh, M.; Chesko, J.; Kazzaz, J.; Soewanan, E.; Ugozzoli, M.; O'Hagan, D. A Practical Approach to the Use of Nanoparticles for Vaccine Delivery. *J. Pharm. Sci.* **2006**, *95*, 2738–2750.
37. Demento, S. L.; Siefert, A. L.; Bandyopadhyay, A.; Sharp, F. A.; Fahmy, T. M. Pathogen-Associated Molecular Patterns on Biomaterials: A Paradigm for Engineering New Vaccines. *Transl. Biotechnol.* **2011**, *29*, 294–306.
38. Krishnamachari, Y.; Salem, A. K. Innovative Strategies for Co-delivering Antigens and CpG Oligonucleotides. *Adv. Drug Delivery Rev.* **2009**, *61*, 205–217.
39. Shen, Z.; Reznikoff, G.; Dranoff, G.; Rock, K. L. Cloned Dendritic Cells Can Present Exogenous Antigens on Both

MHC Class I and Class II Molecules. *J. Immunol.* **1997**, *158*, 2723–2730.

40. West, M. A.; Bretscher, M. S.; Watts, C. Distinct Endocytic Pathways in Epidermal Growth Factor-Stimulated Human Carcinoma A431 Cells. *J. Cell Biol.* **1989**, *109*, 2731–2739.

41. Aoki, T. Tyrosine Phosphorylation of Caveolin-1 in the Endothelium. *Exp. Cell Res.* **1999**, *253*, 629–636.

42. Wang, L. H.; Rothberg, K. G.; Anderson, R. G. Misassembly of Clathrin Lattices on Endosomes Reveals a Regulatory Switch for Coated Pit Formation. *J. Cell Biol.* **1993**, *123*, 1107–1117.

43. Sallusto, F.; Cella, M.; Danielli, C.; Lanzavecchia, A. Dendritic Cells Use Macropinocytosis and the Mannose Receptor To Concentrate Macromolecules in the Major Histocompatibility Complex Class II Compartment: Downregulation by Cytokines and Bacterial Products. *J. Exp. Med.* **1995**, *182*, 389–400.

44. Sandgren, K. J.; Wilkinson, J.; Miranda-Saksena, M.; McInerney, G. M.; Byth-Wilson, K.; Robinson, P. J.; Cunningham, A. L. A Differential Role for Macropinocytosis in Mediating Entry of the Two Forms of Vaccinia Virus Into Dendritic Cells. *PLoS Pathog.* **2010**, *6*, e1000866.

45. Burgdorf, S.; Kurts, C. Endocytosis Mechanisms and the Cell Biology of Antigen Presentation. *Curr. Opin. Immunol.* **2008**, *20*, 89–95.

46. Akin, A.; Langer, R. Measuring the pH Environment of DNA Delivered Using Nonviral Vectors: Implications for Lysosomal Trafficking. *Biotechnol. Bioeng.* **2002**, *78*, 503–508.

47. Accapezzato, D. Chloroquine Enhances Human CD8+ T Cell Responses Against Soluble Antigens *in Vivo*. *J. Exp. Med.* **2005**, *202*, 817–828.

48. Martin, R. M.; Brady, J. L.; Lew, A. M. The Need for IgG2c Specific Antiserum When Isotyping Antibodies from C57BL/6 and NOD Mice. *J. Immunol. Methods* **1998**, *212*, 187–192.

49. Maubant, S.; Banissi, C.; Beck, S.; Chauvat, A.; Carpentier, A. F. Adjuvant Properties of Cytosine-Phosphate-Guanosine Oligodeoxynucleotide in Combination with Various Polycations in an Ovalbumin-Vaccine Model. *Nucleic Acid Ther.* **2011**, *21*, 231–240.

50. Lührs, P.; Schmidt, W.; Kutil, R.; Buschle, M.; Wagner, S. N.; Stingl, G.; Schneeberger, A. Induction of Specific Immune Responses by Polycation-Based Vaccines. *J. Immunol.* **2002**, *169*, 5217–5226.

51. Matzelle, M. M.; Babensee, J. E. Humoral Immune Responses to Model Antigen Co-delivered with Biomaterials Used in Tissue Engineering. *Biomaterials* **2004**, *25*, 295–304.

52. Wegmann, F.; Gartlan, K. H.; Harandi, A. M.; Brinckmann, S. A.; Coccia, M.; Hillson, W. R.; Kok, W. L.; Cole, S.; Ho, L.-P.; Lambe, T.; et al. Polyethyleneimine Is a Potent Mucosal Adjuvant for Viral Glycoprotein Antigens. *Nat. Biotechnol.* **2012**, *30*, 883–888.

53. Amorij, J.-P.; Kersten, G. F. A.; Saluja, V.; Tonnis, W. F.; Hinrichs, W. L. J.; Slüter, B.; Bal, S. M.; Bouwstra, J. A.; Huckriede, A.; Jiskoot, W. Towards Tailored Vaccine Delivery: Needs, Challenges and Perspectives. *J. Controlled Release* **2012**, *161*, 363–376.

54. Reed, S. G.; Bertholet, S.; Coler, R. N.; Friede, M. New Horizons in Adjuvants for Vaccine Development. *Trends Immunol.* **2009**, *30*, 23–32.

55. Vollmer, J.; Krieg, A. M. Immunotherapeutic Applications of CpG Oligodeoxynucleotide TLR9 Agonists. *Adv. Drug Delivery Rev.* **2009**, *61*, 195–204.

56. Sablan, B. P.; Kim, D. J.; Barzaga, N. G.; Chow, W. C.; Cho, M.; Ahn, S. H.; Hwang, S. G.; Lee, J. H.; Namini, H.; Heyward, W. L. Demonstration of Safety and Enhanced Seroprotection Against Hepatitis B with Investigational HBsAg-1018 ISS Vaccine Compared to a Licensed Hepatitis B Vaccine. *Vaccine* **2012**, *30*, 2689–2696.

57. Nierkens, S.; den Brok, M. H.; Sutmuller, R. P. M.; Grauer, O. M.; Bennink, E.; Morgan, M. E.; Fidgor, C. G.; Ruers, T. J. M.; Adema, G. J. *In Vivo* Colocalization of Antigen and CpG within Dendritic Cells Is Associated with the Efficacy of Cancer Immunotherapy. *Cancer Res.* **2008**, *68*, 5390–5396.

58. Cho, H. J.; Takabayashi, K.; Cheng, P. M.; Nguyen, M. D.; Corr, M.; Tuck, S.; Raz, E. Immunostimulatory DNA-Based Vaccines Induce Cytotoxic Lymphocyte Activity by a T-Helper Cell-Independent Mechanism. *Nat. Biotechnol.* **2000**, *18*, 509–514.

59. Lee, J.; Sohn, J. W.; Zhang, Y.; Leong, K. W.; Pisetky, D.; Sullenger, B. A. Nucleic Acid-Binding Polymers as Anti-inflammatory Agents. *Proc. Natl. Acad. Sci. U.S.A.* **2011**, *108*, 14055–14060.

60. Chen, H. C.; Sun, B.; Tran, K. K.; Shen, H. Effects of Particle Size on Toll-like Receptor 9-Mediated Cytokine Profiles. *Biomaterials* **2011**, *32*, 1731–1737.

61. Honda, K.; Ohba, Y.; Yanai, H.; Negishi, H.; Mizutani, T.; Takaoka, A.; Taya, C.; Taniguchi, T. Spatiotemporal Regulation of MyD88-IRF-7 Signalling for Robust Type-I Interferon Induction. *Nature* **2005**, *434*, 1035–1040.

62. Paludan, C.; Schmid, D.; Landthaler, M.; Vockerodt, M.; Kube, D.; Tuschl, T.; Münz, C. Endogenous MHC Class II Processing of a Viral Nuclear Antigen After Autophagy. *Science* **2005**, *307*, 593–596.

63. Schmid, D.; Pypaert, M.; Münz, C. Antigen-Loading Compartments for Major Histocompatibility Complex Class II Molecules Continuously Receive Input from Autophagosomes. *Immunity* **2007**, *26*, 79–92.

64. Dengjel, J.; Schoor, O.; Fischer, R.; Reich, M.; Kraus, M.; Müller, M.; Kreymborg, K.; Altenberend, F.; Brandenburg, J.; Kalbacher, H.; et al. Autophagy Promotes MHC Class II Presentation of Peptides from Intracellular Source Proteins. *Proc. Natl. Acad. Sci. U.S.A.* **2005**, *102*, 7922–7927.

65. Lee, H. K.; Lund, J. M.; Ramanathan, B.; Mizushima, N.; Iwasaki, A. Autophagy-Dependent Viral Recognition by Plasmacytoid Dendritic Cells. *Science* **2007**, *315*, 1398–1401.

66. Bertin, S.; Pierrefite-Carle, V. Autophagy and Toll-like Receptors: A New Link in Cancer Cells. *Autophagy* **2008**, *4*, 1086–1089.

67. Combadiere, B.; Liard, C. Transcutaneous and Intradermal Vaccination. *Hum. Vaccines* **2011**, *7*, 811–827.

68. Romani, N.; Flacher, V.; Tripp, C. H.; Sparber, F.; Ebner, S.; Stoitzner, P. Targeting Skin Dendritic Cells To Improve Intradermal Vaccination. *Curr. Top. Microbiol. Immunol.* **2012**, *351*, 113–138.

69. Mohanan, D.; Slüter, B.; Henriksen-Lacey, M.; Jiskoot, W.; Bouwstra, J. A.; Perrie, Y.; Kündig, T. M.; Gander, B.; Johansen, P. Administration Routes Affect the Quality of Immune Responses: A Cross-Sectional Evaluation of Particulate Antigen-Delivery Systems. *J. Controlled Release* **2010**, *147*, 342–349.

70. Eby, J. K.; Dane, K. Y.; O’Neil, C. P.; Hirosue, S.; Swartz, M. A.; Hubbell, J. A. Polymer Micelles with Pyridyl Disulfide-Coupled Antigen Travel through Lymphatics and Show Enhanced Cellular Responses Following Immunization. *Acta Biomater.* **2012**, *8*, 3210–3217.

71. Sheng, K.-C.; Kalkanidis, M.; Pouliotis, D. S.; Espanol, S.; Tang, C. K.; Apostolopoulos, V.; Pietersz, G. A. Delivery of Antigen Using a Novel Mannosylated Dendrimer Potentiates Immunogenicity *in Vitro* and *in Vivo*. *Eur. J. Immunol.* **2008**, *38*, 424–436.

72. Kar, U. K.; Jiang, J.; Champion, C. I.; Salehi, S.; Srivastava, M.; Sharma, S.; Rabizadeh, S.; Niazi, K.; Kickhoefer, V.; Rome, L. H.; et al. Vault Nanocapsules as Adjuvants Favor Cell-Mediated over Antibody-Mediated Immune Responses Following Immunization of Mice. *PLoS One* **2012**, *7*, e38553.

73. Bulmus, V.; Woodward, M.; Lin, L.; Murthy, N.; Stayton, P.; Hoffman, A. A New pH-Responsive and Glutathione-Responsive, Endosomal Membrane-Disruptive Polymeric Carrier for Intracellular Delivery of Biomolecular Drugs. *J. Controlled Release* **2003**, *93*, 105–120.

74. Murthy, N.; Campbell, J.; Fausto, N.; Hoffman, A. S.; Stayton, P. S. Bioinspired pH-Responsive Polymers for the Intracellular Delivery of Biomolecular Drugs. *Bioconjugate Chem.* **2003**, *14*, 412–419.

75. Broaders, K. E.; Cohen, J. A.; Beaudette, T. T.; Bachelder, E. M.; Fréchet, J. M. J. Acetalated Dextran Is a Chemically

and Biologically Tunable Material for Particulate Immunotherapy. *Proc. Natl. Acad. Sci. U.S.A.* **2009**, *106*, 5497–5502.

76. Karttunen, J.; Sanderson, S.; Shastri, N. Detection of Rare Antigen-Presenting Cells by the LacZ T-Cell Activation Assay Suggests an Expression Cloning Strategy for T-Cell Antigens. *Proc. Natl. Acad. Sci. U.S.A.* **1992**, *89*, 620–624.

77. Belizaire, R.; Unanue, E. R. Targeting Proteins to Distinct Subcellular Compartments Reveals Unique Requirements for MHC Class I and II Presentation. *Proc. Natl. Acad. Sci. U.S.A.* **2009**, *106*, 17463–17468.

78. Schwarz, K.; de Giuli, R.; Schmidtke, G.; Kostka, S.; van den Broek, M.; Kim, K. B.; Crews, C. M.; Kraft, R.; Groettrup, M. The Selective Proteasome Inhibitors Lactacystin and Epoxomicin Can Be Used To Either Up- or Down-Regulate Antigen Presentation at Nontoxic Doses. *J. Immunol.* **2000**, *164*, 6147–6157.

79. Gerelchuluun, T.; Lee, Y.-H.; Lee, Y.-R.; Im, S.-A.; Song, S.; Park, J. S.; Han, K.; Kim, K.; Lee, C.-K. Dendritic Cells Process Antigens Encapsulated in a Biodegradable Polymer, Poly-(D,L-lactide-co-glycolide), via an Alternate Class I MHC Processing Pathway. *Arch. Pharmacol. Res.* **2007**, *30*, 1440–1446.

80. Murthy, N.; Robichaud, J. R.; Tirrell, D. A.; Stayton, P. S.; Hoffman, A. S. The Design and Synthesis of Polymers for Eukaryotic Membrane Disruption. *J. Controlled Release* **1999**, *61*, 137–143.

81. De Koker, S.; De Geest, B. G.; Singh, S. K.; De Rycke, R.; Naessens, T.; van Kooyk, Y.; Demeester, J.; De Smedt, S. C.; Grootenhuis, J. Polyelectrolyte Microcapsules as Antigen Delivery Vehicles to Dendritic Cells: Uptake, Processing, and Cross-Presentation of Encapsulated Antigens. *Angew. Chem., Int. Ed.* **2009**, *48*, 8485–8489.

82. Brito, L. A.; Singh, M. Acceptable Levels of Endotoxin in Vaccine Formulations During Preclinical Research. *J. Pharm. Sci.* **2010**, *100*, 34–37.